Applied Physics A (2018) 124:237
https://doi.org/10.1007/s00339-018-1663-9

Applied Physics A
Materials Science & Processing

Nanosecond laser ablation of target Al in a gaseous medium: explosive boiling

V. I. Mazhukin[1,2] · A. V. Mazhukin[1,2] · M. M. Demin[1] · A. V. Shapranov[1,2]

Received: 3 November 2017 / Accepted: 7 February 2018 / Published online: 12 February 2018

Abstract
An approximate mathematical description of the processes of homogeneous nucleation and homogeneous evaporation (explosive boiling) of a metal target (Al) under the influence of ns laser radiation is proposed in the framework of the hydrodynamic model. Within the continuum approach, a multi-phase, multi-front hydrodynamic model and a computational algorithm are designed to simulate nanosecond laser ablation of the metal targets immersed in gaseous media. The proposed approach is intended for modeling and detailed analysis of the mechanisms of heterogeneous and homogeneous evaporation and their interaction with each other. It is shown that the proposed model and computational algorithm allow modeling of interrelated mechanisms of heterogeneous and homogeneous evaporation of metals, manifested in the form of pulsating explosive boiling. Modeling has shown that explosive evaporation in metals is due to the presence of a near-surface temperature maximum. It has been established that in nanosecond pulsed laser ablation, such exposure regimes can be implemented in which phase explosion is the main mechanism of material removal.

1 Introduction

The increased interest in pulsed laser ablation (PLA) [1–3] is primarily due to the increasing possibilities of its use in many applications: microprocessing [4], pulse laser deposition (PLD) [5], laser-induced breakdown spectroscopy (LIBS) [6] production of nanomaterials [7], laser synthesis of colloids [8], biomedicine [9, 10].

Numerous applications make PLA an attractive field for basic research. Despite extensive studies of the fundamental properties of laser ablation performed earlier, a number of important physical phenomena still remain insufficiently well investigated and understood.

The greatest differences in the physical mechanisms of laser ablation of metals are observed between the short (ns) and ultrashort (ps, fs) pulse action [11, 12].

In the ultrashort range (fs, ps) of laser action, laser radiation freely reaches the surface of the target. The absorption of laser radiation by a degenerate electron gas, followed by a slowed-down energy exchange between the electron and phonon components, leads to a strong deviation from the locally thermodynamic equilibrium of the system as a whole. As a result, laser ablation and its accompanying processes develop after the end of the pulse.

Laser ablation of condensed media with short nanosecond pulses initiates a complex sequence of processes that occur both during and after the end of the laser pulse. In the nanosecond range, under a certain choice of the exposure regimes, in contrast to the ultrashort fs, ps-action, two phenomena are clearly observed experimentally and investigated—volumetric evaporation (phase explosion) of the liquid phase of the target [13–19] and formation of a long-lived laser plasma in the evaporated substance and the surrounding gas [20–23].

In spite of the fact that previously the action of nanosecond laser pulses on metals has been studied in a number of experimental and theoretical studies [15, 16, 24], a number of important physical processes underlying ablation are still poorly understood due to their complexity. The presence of a large number of interrelated physical processes makes it difficult to experimentally determine and study the basic mechanisms of ablation. The most complex and least studied of them are the mechanisms of homogeneous phase transitions in the vicinity of the critical point [13–19]. For this reason, nanosecond laser ablation continues to be an active

✉ V. I. Mazhukin
vim@modhef.ru

[1] Keldysh Institute of Applied Mathematics, RAS, Miusskaya sq., 4, Moscow, Russia

[2] National Research Nuclear University "MEPhI", Kashirskoe shosse, 31, Moscow, Russia

area of research in which mathematical modeling plays an increasingly important role [25–27].

Various theoretical approaches are used for the mathematical description and analysis of the PLA process of the condensed media: continuum, kinetic, atomistic (molecular-dynamic), etc. Each of them has its own field of applicability, its advantages and disadvantages.

Atomistic models allow us to conduct research at the atomic level and obtain fundamental knowledge about the structure, thermodynamic and mechanical properties of crystalline materials [28, 29], the physical mechanisms of various processes [30, 31], including the kinetics of heterogeneous and homogeneous phase transitions [32, 33]. The basic methods of atomistic modeling—molecular dynamics (MD) and Monte Carlo (MC), which use, as a rule, semiempirical interaction potentials, operate with tens and hundreds of millions of atoms and allow calculations in the time range of nanosecond duration. However, even with the use of high-performance computing platforms, the computational costs are enormous and often a number of PLA processes, because of their inherent strong spatial–temporal scaling, are beyond the reach of atomistic modeling methods. Therefore, in spite of constant progress in the field of designing interatomic potentials and increasing the power of computing systems, the final overcoming of computational constraints is hardly achievable, and continual models will always remain important.

Continuum models based on the equations of continuum mechanics form a class of widely used hydrodynamic models [25–27, 34–36], use minimum information and operate with average values of physical characteristics calculated from an infinitesimal volume. The methods for solving them are more compact, they have higher accuracy and a relatively small amount of computation. The main shortcomings of the continuum approach are manifested in the absence of the possibility of direct investigation of elementary processes in materials, and there are great difficulties in the mathematical description of homogeneous melting/crystallization and evaporation mechanisms, as well as limited possibilities for calculating thermophysical, thermodynamic, optical and other characteristics of the substance in a wide range of parameters. These problems are much easier and more fully solved within the framework of atomistic modeling, the results of which can then be used in the form of input parameters in meso- and macrolevel models.

The proposed work considers the application of the continuum approach to modeling of dynamics and the main mechanisms of the ns-PLA of the metal (Al) target in air in the preplasma regime.

The main goal of the work is to develop an approximate mathematical description of homogeneous nucleation and homogeneous evaporation of a metal (Al) target under the influence of ns laser radiation within the framework of the hydrodynamic model. The proposed approach is used for modeling and detailed analysis of the mechanisms of heterogeneous and homogeneous evaporation and their interaction with each other.

2 Mathematical formulation and algorithm of solution

Mathematical description of ns-PLA involving processes in the condensed (target) and vapor–gas (vaporized matter, gas) medium is realized by a system of nonstationary equations of gas-hydrodynamics, equations of energy with thermal conductivity, and equations of transfer of laser radiation. Equations are supplemented by the corresponding equations of state.

Assumptions and limitations It is assumed that the radius of the focal spot of the laser r_f is significantly larger than the thermal influence depth ℓ_T in the target: $r_f \gg \ell_T$; in the gaseous medium, the characteristic time for the consideration of the processes $t_1 \leqslant t_0$ does not exceed the propagation time of the perturbation from the center of the ray $t_0 = r_f/u_{sw}$ that allows us to ignore edge effects and use 1-D approximation in the spatial variable x; The duration of the laser pulse $\tau \geq 5$ ns in the considered regimes of laser action is sufficient to fulfill the conditions of locally thermodynamic equilibrium (LTE), which allows using the one-temperature approximation.

The right boundary $\Gamma_g(t)$, propagating over unperturbed air, is made moving with the purpose of increasing the efficiency of the computational algorithm. The scheme of the boundaries and their movement direction are plotted at Fig. 1.

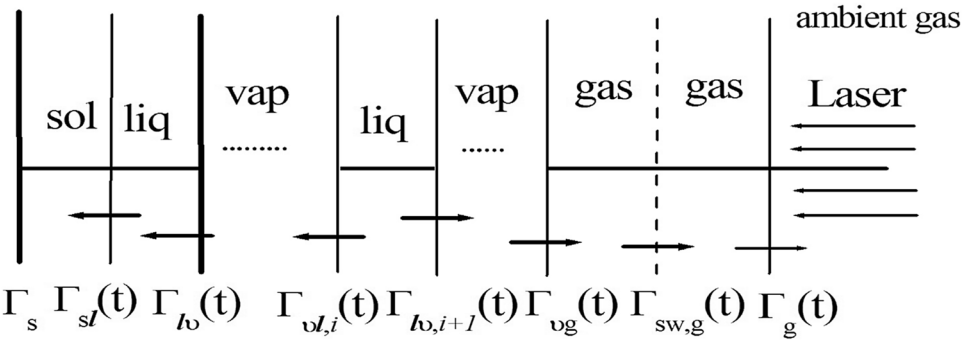

Fig. 1 Scheme of the spatial position of the phases and the direction of motion of the interphase and contact boundaries, and the front of the shock wave

The phase states and the vapor–gas medium are separated by moving interphase boundaries: in the target solid–liquid $\Gamma_{s\ell}(t)$, liquid–vapor $\Gamma_{\ell\upsilon}(t)$; in the fragment $\Gamma_{\ell\upsilon,i}(t)$; and contact boundary $\Gamma_{\upsilon g}(t)$ and shock wave $\Gamma_{sh,g}(t)$.

2.1 Hydrodynamic model

A complete system of equations is written in the following form:

$$\left[\begin{array}{l} \frac{\partial\rho}{\partial t}+\frac{\partial(\rho u)}{\partial x}=0, \\ \frac{\partial(\rho u)}{\partial t}+\frac{\partial(\rho u^2)}{\partial x}+\frac{\partial p}{\partial x}=0, \\ \frac{\partial(\rho\varepsilon)}{\partial t}+\frac{\partial(\rho u\varepsilon)}{\partial x}=-\left(p\frac{\partial u}{\partial x}+\frac{\partial W_T}{\partial x}+\frac{\partial G}{\partial x}\right), \\ \frac{\partial G}{\partial x}+\kappa(\rho,T)G=0, \\ W_T=-\lambda(T)\frac{\partial T}{\partial x} \\ p=p(\rho,T), \quad \varepsilon=\varepsilon(\rho,T) \end{array}\right]_k \quad k=s,\ell,\upsilon,g$$

$$-t_0\leqslant t<\infty, \quad \left\{\begin{array}{l} \Gamma_s<x<\Gamma_{s\ell}(t)\cup\Gamma_{s\ell}(t)<x<\Gamma_{\ell\upsilon}(t)\cup\cdots\Gamma_{\ell\upsilon,i}(t)<x<\Gamma_{\ell\upsilon,i+1}(t)\cdots \\ \quad\cup\Gamma_{\ell\upsilon,i+1}(t)<x<\Gamma_{\upsilon g}(t)\cup\Gamma_{\upsilon g}(t)<x<\Gamma_{sw,g}(t)\cup\Gamma_{sw,g}(t)<x<\Gamma_g(t) \end{array}\right\}.$$

Here ρ, u, ε, T, p are the density, gas-dynamic velocity, internal energy, temperature and pressure correspondingly, κ and G are the absorption coefficient and laser flow density, W_T is the heat flow density, λ is the heat conductivity coefficient. The indexes s, ℓ, υ, g signify solid, liquid, vapor and gaseous (air) medium. In the condensed phase, ε_k has the meaning of enthalpy of solid and liquid phases H_k.

A distinctive feature of heterogeneous phase transitions is the presence of the sharp interphase interfaces $\Gamma_{s\ell}(t)$ and $\Gamma_{\ell\upsilon}(t)$, where the main thermophysical and optical properties have a break: enthalpy H, the coefficients of specific heat C_p and heat conductivity λ, density ρ, pressure p и surface reflectivity R.

For fast phase transitions that are typical for the ns–PLA, the models describing the mechanisms of heterogeneous melting and evaporation are the systems of equations at the corresponding interphase boundary ($\Gamma_{s\ell}(t)$, $\Gamma_{\ell\upsilon}(t)$) and expressing three conservation laws: mass, momentum and energy. These equations are supplemented by the corresponding kinetic relations characterizing the degree of nonequilibrium of the phase transition. For the melting/crystallization process, this condition is the kinetic expression for the velocity of motion of the melting front $\upsilon_{s\ell}$ [37, 38]. The model of heterogeneous evaporation/condensation is characterized by the presence of a thin (several path lengths) nonequilibrium Knudsen layer (KL) adjacent to the interface surface of the phases $\Gamma_{\ell\upsilon}(t)$. The degree of nonequilibrium of the phase transition in this model is determined by Mach number ($M=u_\upsilon/u_{sound}$) at the outer side of KL.

A complete and detailed description of the models of heterogeneous melting/crystallization and evaporation/condensation is given in [39], and therefore is absent in this paper.

2.2 Computational algorithm

The presence of moving interphase and contact boundaries, as well as fronts of discontinuous solutions (shock waves, fragments of condensed matter), zones of large gradients and their rapid propagation through space, imposes strict requirements on the effectiveness of the computational algorithms used and in the first place, not to the quality of difference schemes, but rather to the principles of constructing optimal computational grids. The differential model (1) that included the equations of gas-dynamics, equations of energy with non-linear thermal conductivity and radiation transport was approximated by a family of conservative finite-difference schemes [40, 41] written on the computational grids with dynamic adaptation [42, 43]. The method of dynamic adaptation is based on the idea of transition to an arbitrary nonstationary coordinate system which velocity is not known beforehand and is determined by a coordinate transformation using the sought solution. The use of an arbitrary nonstationary coordinate system allows the problem of constructing and adapting computational grids to be formulated at the differential level, i.e. in the resulting mathematical model, part of the differential equations describes the physical processes, and the other—the behavior of the grid nodes. In addition, the transition to an arbitrary nonstationary coordinate system makes it possible to perform calculations with an arbitrary number of discontinuous solutions, such as shock waves, propagating phase and temperature fronts, contact boundaries and ejected fragments. The efficiency of the method is determined by the complete matching of the speed of movement of grid nodes with the dynamics of the solution, which makes it possible to reduce their number by 2–3 orders of magnitude in comparison with grids with fixed nodes.

In the problem under consideration, a typical calculation contained the total number of nodes of the order of $(8–10)\times10^2$, (depending on the number of the fragments taken into account, 10–70). Of these nodes, $(1–2)\times10^2$

accounted for the condensed and vapor–gas medium, 25–30 nodes were allocated to each of the fragments and the cavities of the vapor between them.

3 Modeling and analysis of results

One of the purposes of this work is a detailed study of the mechanism of explosive boiling in metals, since explosive boiling is considered to be the most efficient thermal mechanism for laser ablation of materials. At the same time, difficulties associated with understanding the mechanism of homogeneous phase transitions in metals occurring under the action of ns-laser pulses are known. At present, there is no doubt about the connection between the mechanism of volume removal of matter and the occurrence of a subsurface temperature maximum in weakly absorbing liquids and non-metallic solid materials exposed to laser radiation. The validity of this statement was confirmed by the results of mathematical modeling based on the thermal model by a number of authors, [16, 44]. For strongly absorbing media, mainly metallic, calculations based on the thermal model [16, 19] have shown that the magnitude of the near-surface temperature maximum is several degrees. On this basis, overheating was excluded from consideration, up to the statement that in metals the maximum temperature is always on the surface of the target, and subsurface overheating is impossible. Explosive boiling was interpreted as a surface spray of the liquid phase when the critical temperature is reached at the surface [13, 14]. This interpretation is not convincing, since it does not allow us to formulate non-contradictory ideas about the mechanism of homogeneous evaporation of metals, including the explosive boiling process with the formation of nanocavities under the ns-laser action.

Let us consider the ns-PLA process of Al target with thickness of 100 μm, placed in the gaseous medium at the normal conditions $p=1$ bar и $T=300$ K. Laser radiation propagates from the right to the left and the pulse has Gauss shape: $G=(\beta/\pi)^{1/2}G_0\cdot\exp(-\beta(t/\tau)^2)$, where $\infty<t<\infty$, $\tau=5\times10^{-9}$ s is the full width at half maximum, and the wavelength $\lambda_L=1.06$ μm and fluence of $F=5.2$ J cm^{-2}. Here $G_0=1.04\times10^9$ W cm^{-2} is the peak intensity at $t=0$, $\beta=4\times\ln 2$. For these parameters, the start moment of time was $t=-t_0=-4\tau$. The air for the selected exposure mode is completely transparent to the laser radiation, which is partially reflected from the metal surface, and partially absorbed in the target.

Modeling of the processes of laser heating, melting, surface evaporation, and evolution of the plume in the gas–vapor medium is performed within the framework of the hydrodynamic model, taking into account the temperature dependence of the material properties of the target and the explicit tracking of fronts of all moving boundaries (interphase, contact and shock waves).

Figure 2a–c shows temperature dependencies of thermophysical $C_p(T)$, $\lambda(T)$, $L_v(T)$, and optical $\kappa(T)$ properties of Al. The curves of $L_v(T)$ and $C_p(T)$ are obtained from molecular-dynamic calculations, $\lambda(T)$, $\kappa(T)$, $R(T)$ are constructed based on theoretical concepts [45–47] and reference data [48].

3.1 The stage of heterogeneous evaporation

At the initial stage of the laser action at relatively low temperatures $T\ll T_{cr}$, the optical properties of Aluminum for the near infrared radiation are in the range $k\geq10^7$ m^{-1} and $R(T_{sur})\approx0.95$–0.6. When the duration of the acting pulse is $\tau_L\geq10^{-7}$ s, the conditions for the surface release of energy are fulfilled meaning that the heat action length ℓ_T is significantly larger that free path of the energy quantum ℓ_r, i.e., $\ell_t\approx(at)^{1/2}\gg\ell_r\approx k^{-1}$.

Surface energy release determines the heterogeneous character of the heating and phase transformations in the target. Appearance of the phase fronts of melting and evaporation in the target, the fronts of the contact boundary and the shock wave in the gaseous medium, and also the formation of new regions of the liquid and vapor phases associated with them, occur at the leading edge of the laser pulse. Heterogeneous melting starts at the time of $t=-2.3\times10^{-9}$ s and during short time up to $t=-2.1\times10^{-9}$ s the velocity of the melting front reaches the maximum value of $v_{s\ell}=250$ m s^{-1}. The formed front of surface melting $\Gamma_{s\ell}(t)$ propagates deep into the target, forming a new region of the liquid phase. Further heating results in the appearance (at the moment of $t=-1.8\times10^{-9}$ s), of the heterogeneous evaporation front $\Gamma_{\ell v}(t)$, propagating inside the melt. The maximum velocity of the evaporation front $v_{\ell v}=23$ m s^{-1} reached at the time of $t=-0.9\times10^{-9}$ s, is approximately 10 times lower than that of the melting front $v_{s\ell}$. Surface evaporation begins when the following relation for pressures $p_{sat}(t)$ and $p_g(t)$ starts to be valid: $p_{sat}(t)>p_g(t)$. The process is controlled by the surface temperature $T_{sur}(t)$ and Mach number $M(t)$ at the outer side of the KL, $(0<M(t)\leq1)$. Near the surface of the melt, a stream of evaporated matter is formed, which, by pushing the air, forms a new area occupied by the vapor and bounded from the two sides by the moving boundaries: interphase $\Gamma_{\ell v}(t)$ and contact $\Gamma_{vg}(t)$—vapor/air (Fig. 3).

The flow of the evaporated substance, acting like a piston, pushes out the cold air and, after doing a certain job, warms up to a temperature $T_{vap}=4.4\times10^3$ K. Under the pushing action of hot vapor, compression of the cold dense air occurs, which at the moment of $t=-1.6\times10^{-9}$ s turns into a shock wave with the front $\Gamma_{sh,g}(t)$. As a result, an expanding region of air heated by the forces of gas-dynamic compression is formed between the moving boundaries $\Gamma_{vg}(t)$ and $\Gamma_{sw,g}(t)$. The spatial structure of the erosion plume after the

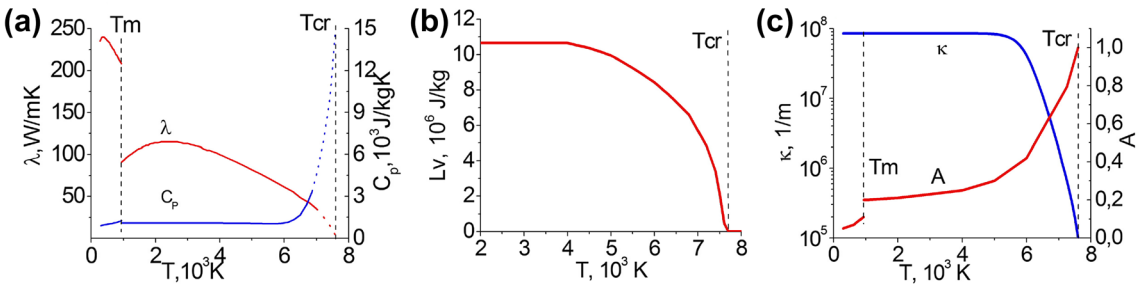

Fig. 2 **a–c** Temperature dependencies of thermophysical $C_p(T)$, $\lambda(T)$, $L_v(T)$, and optical $\kappa(T)$, $A(t)$ properties of Al

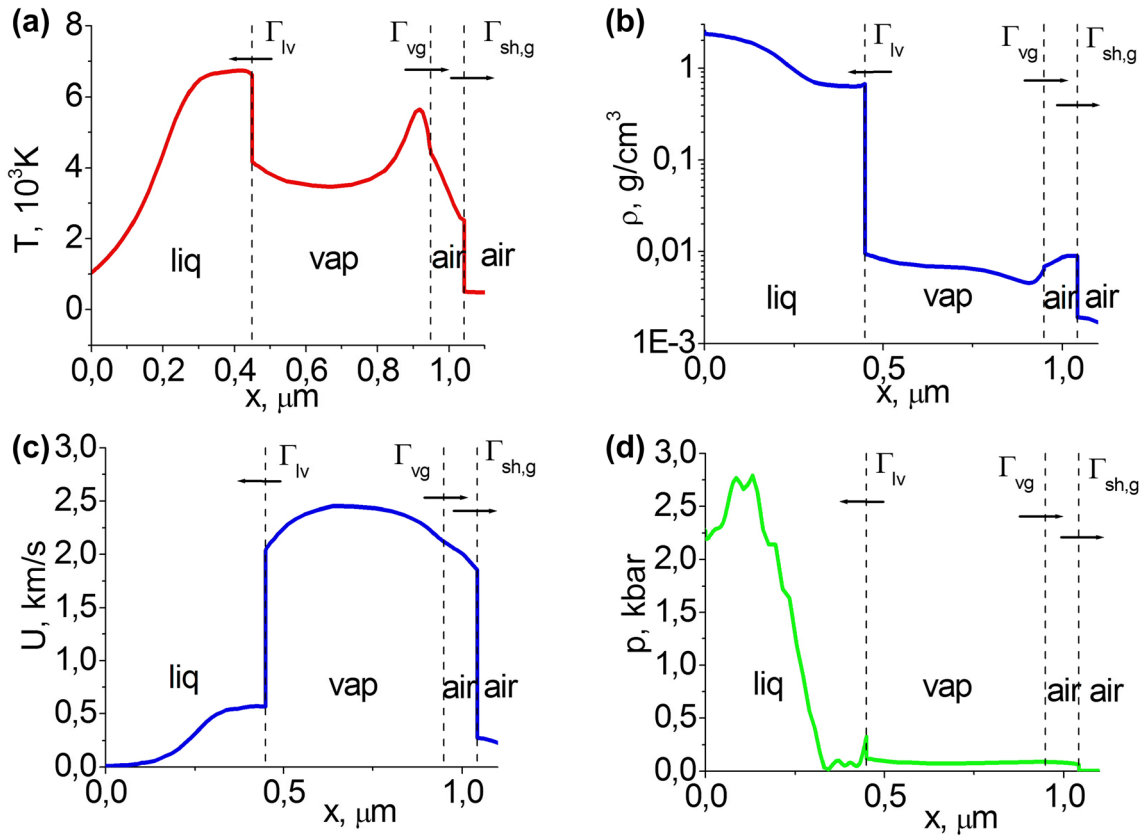

Fig. 3 **a–d** The spatial structure of the plume after the formation of the shock wave $T(x)$, $\rho(x)$, $u(x)$, $p(x)$, $t = -1.3$ ns

formation of the shock wave is represented by the main characteristics $T(x)$, $\rho(x)$, $u(x)$, $p(x)$ at Fig. 3a–d.

Subsequently, the shock wave with increasing velocity $v_{sw,g} = 2.9$ km s^{-1} and temperature $T_{sw,g} = 3.4 \times 10^3$ K propagates toward the laser beam, outrunning the contact boundary moving with a lower velocity ($v_{sw,g} = 2.5$ km s^{-1}) and higher temperature. The temperature of the vapor and air is, in this case, is insufficient for the initiation of ionization, and the vapor–gas medium remains transparent for laser radiation.

Note that the distinctive feature of the mechanisms of heterogeneous heating and phase transformations of the substance (surface heating and evaporation) is the presence of two features: (a) the maximum of the spatial temperature profile $T_{k,max}(x)$ always coincides with the temperature of the melting T_{melt} or evaporating surface T_{sur}; (b) the pressure at the evaporating surface $p_{sur}(T_{sur})$ is always lower than that of the saturated vapor $p_{sat}(T_{sur})$. At the maximum evaporation velocity with $M(t) = 1$ the pressure at the surface reaches its minimum value

$p_{sur}(T_{sur}) \approx 0.55 p_{sat}(T_{sur})$. The surface of the target is in this case in the most superheated metastable state.

3.2 The stage of homogeneous evaporation

The second stage of the development of PLA begins with a qualitative change in the behavior of the processes, which is associated with a change in the surface mechanism of the release of laser energy into a volumetric one and the formation of a subsurface temperature maximum in the target. Rapid heating of the metal target transfers the substance to the region of critical parameters, where the optical and thermophysical properties undergo sharp changes. In the critical region, under the influence of the transparency wave [45, 46], the volume absorption coefficient of Al k decreases by 2–3 orders of magnitude with a simultaneous increase in the absorptivity of surface A to 80–100%. Specific heat C_p increases by 5–7 times and heat conductivity coefficient drops to $\lambda_\ell = 2$ W m^{-1} K^{-1}. When the heterogeneous evaporation front velocity reaches the value of $v_{s\ell} \approx 10$–20 m s^{-1} the condition of volume energy release is satisfied in the substance in the form $ak/v_{\ell v} \ll 1$. The presence of the surface evaporation provides inhomogeneity of the volume heating and contributes to the formation of a subsurface temperature maximum $T_{\ell,max}$, Fig. 4. Figure 4 shows typical values of the maximum overheating $\Delta T = T_{\ell,max} - T_{sur}$ and its depth $\Delta\ell$ in liquid phase of Al for the considered regime of the laser action at the time of $t \sim -0.9 \times 10^{-9}$ s when the temperature maximum $T_{\ell,max}$ reaches its limiting value $T_{lim,max}$. The value of maximum overheating $\Delta T \sim 160$ K is reached at the depth $\Delta\ell \sim 40$ nm. These values are close to corresponding values obtained from the molecular-dynamic simulation [39]. For the overheated metastable liquid layer $\Delta\ell$ adjacent to the surface with temperature profile $T_{\ell,max} \geq T > T_{sur}$ the following relations are met: $p_{sat}(T_{\ell,max}) > p_{sat}(T_{sur}) > p_{sur}(T_{sur})$, testifying that at the point with $T_{\ell,max} = T_{lim,max}$, all conditions for the emergence of a new phase are satisfied.

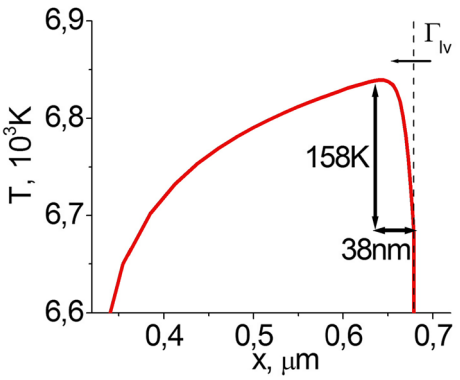

Fig. 4 The fragment of the profile $T(x)$ in the near-surface layer of the target before the first splitting, $t = -0.9$ ns

3.2.1 Algorithm for modeling of explosive boiling

Explosive boiling of the irradiated target occurs when the temperature maximum $T_{\ell,max}$ reaches the value of overheating limit $T_{lim,max}$, which determines the boundary of the absolute instability of the liquid phase of Al at the given external pressure p_{sur}. The driving force of explosive boiling (homogeneous evaporation) is the pressure drop in the region between the temperature maximum and the evaporating surface. In the continuum models, for the mathematical modeling of homogeneous evaporation mechanisms it is proposed to use the procedure for generating artificial quasi-nuclei [49, 50]. The evolution of quasi-nuclei promotes the formation of nanocavities, the growing pressure in which results in the release of thin cooler near-surface layers of liquid into the gas medium. In the 1-D approximation in space, the simulation algorithm for the explosive boiling consists of introduction, under certain criteria, of artificial quasi-nuclei into the superheated liquid phase. Quasi-nuclei have the thickness $h_i(t)$ and are limited by moving interphase boundaries liquid–vapor $x_i(t) = \Gamma_{\ell v,i}(t)$, $x_{i+1}(t) = \Gamma_{\ell v,i+1}(t)$, where $i = 1, 2, \ldots$ is the number of the quasi-nucleus. As a criterion for the beginning of nucleation in the calculations we used the time t_i and spatial coordinate x_i, where the relation $T_{\ell,max}(t_i, x_i) \geq T_{lim,max}$ holds and where then a quasi-nucleus is placed. The values of the maximum temperature for the overheating $T_{lim,max}$ for liquid Al, depending on the heating rate and external counterpressure, were determined from the molecular dynamic modeling [17, 18] and are in the range $T_{lim,max} \approx (0.89$–$0.95) T_{cr}$. The effect of counterpressure was taken into account through the temperature difference $\Delta T = T_{\ell,max} - T_{sur}$, which is determined from the solution of the hydrodynamic model (1).

3.3 Modeling of pulsating explosive boiling

The conditions for the first ejection are satisfied at the moment of $t_1 \approx -0.9 \times 10^{-9}$ s when at the point $\Delta x_1 = 43$ nm the equality $T_{\ell,max} \approx T_{lim,max} = 0.9 \times T_{cr} = 6840$ K is satisfied. The velocity of the evaporation front $v_{\ell v}$ and Mach number M at the outer side of KL reach their maximum values: $v_{\ell v} = 23$ m s^{-1}, $M = 1$. The temperature at the evaporating surface is $T_{sur} \approx 6680$ K. The temperature difference is $\Delta T = T_{\ell,max} - T_{sur} = 160$ K. Accordingly, the saturated vapor pressure for the temperature maximum $p_{sat}(0.9 \times T_{cr}) = 720$ bar is much greater than the pressure on the target surface $p_{sur}(6680\text{ K}) \approx 0.55 p_{sat}(6680\text{ K}) = 344$ bar. The pressure difference in the overheated near-surface layer is $\Delta p = p_{sat} - p_{sur} = 376$ bar. The first quasi-nucleus of the vapor phase with the start thickness $h_1(t) = \Gamma_{\ell v,2}(t) - \Gamma_{\ell v,1}(t) \sim 5$ nm, is placed at the point of the near-surface temperature maximum $x = x_1$. The description of the processes in the expanding cavity and near-surface layer of the liquid

separated from the main target is realized by means of the gas-hydrodynamic system of equations (1). The model of heterogeneous evaporation [39] is used as the boundary conditions at the interphase planes $\Gamma_{\ell v,1}(t)$, $\Gamma_{\ell v,2}(t)$ with account of reflection and absorption of laser radiation in the formed layer. The initial conditions for a new region of vapor bounded by 2 flat surfaces were given in the form

$$T_{v,1} = T_{v,2} = T_{\ell,\max}, \quad p_{v,1} = p_{v,2} = p_{\text{sat}}(T_{\ell,\max}).$$

Under the influence of the excess pressure Δp and the effects of heterogeneous evaporation, the formation of a rapidly expanding cavity filled with vapor takes place followed by the ejection of a layer of liquid with the thickness $d_1(t) = \Gamma_{\ell v,1}(t) - \Gamma_{\ell v}(t) \approx 43$ nm towards the gaseous medium and followed by the formation of a new liquid/vapor interface.

In the case of repeated explosive boiling with the formation of the next liquid fragment for each of them, as well as the main target, the gaseous medium and the formed vapor cavities, the solution algorithm remains unchanged. An additional circumstance is only the need to take into account the inhibitory effect from the previously split fragment. If the first explosive boiling occurs at low external pressure ($p = 1$ bar), which does not have a noticeable effect on the process of heterogeneous evaporation, then during repeated explosive boiling the liquid phase to be ejected must overcome the high pressure (several hundred bar) of the previously evaporated substance. The greatest influence is exerted by the counter pressure on the conditions for the formation of the maximum temperature in the near-surface layer and the thickness of the detached fragment of the liquid phase. Because of the noticeable reduction of the heterogeneous evaporation rate ($M \approx 0.32$) at the target and

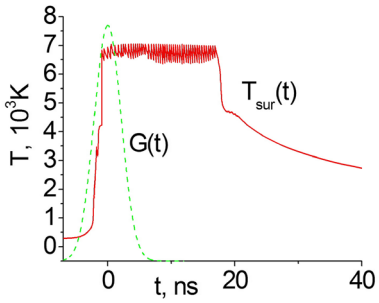

Fig. 6 Time dependence of the surface temperature $T_{\text{sur}}(t)$ due to explosive boiling

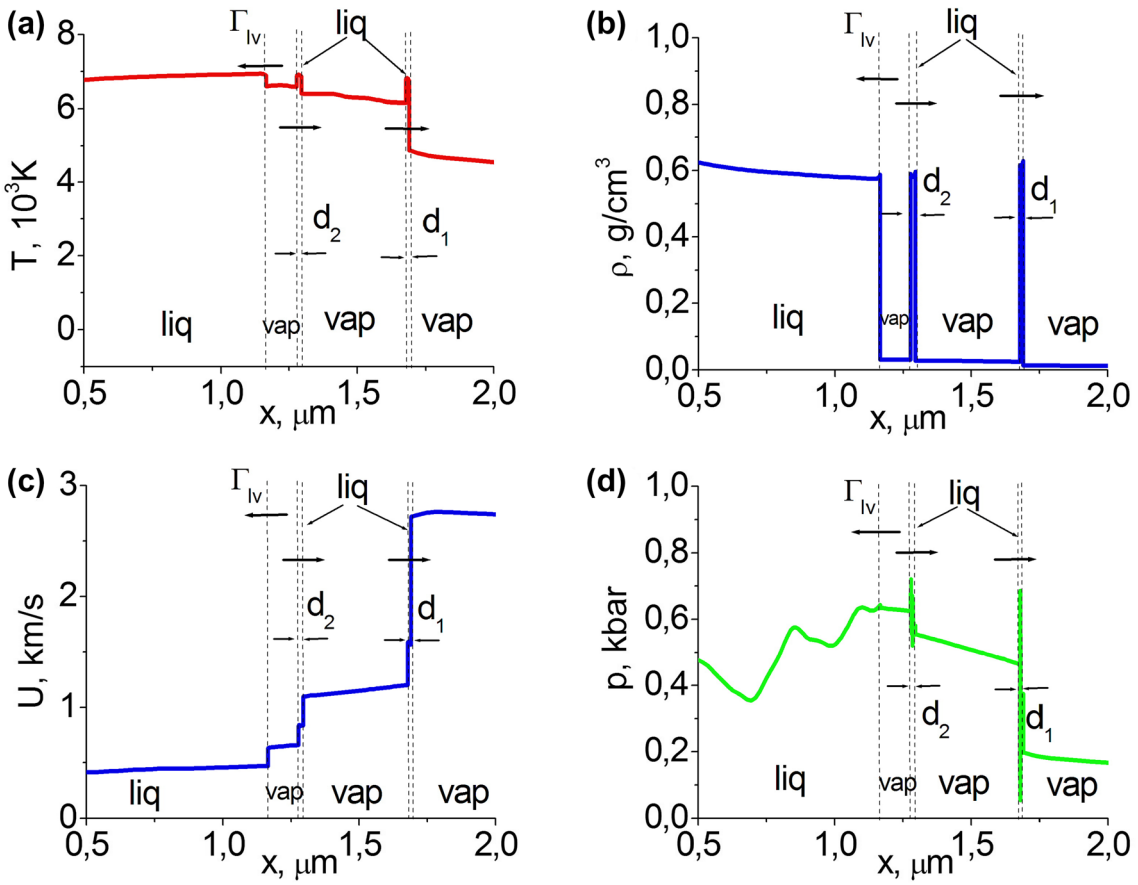

Fig. 5 The partial profiles with two ejected fragments of liquid in the vapor phase at time $t = -0.1$ ns: **a** $T(x)$; **b** $\rho(x)$; **c** $U(x)$, **d** $P(x)$

ejected fragment surfaces, new explosive boiling occurs at the moment $t_2 \approx -0.6 \times 10^{-9}$ s when the equality $T_{\ell,\max} \approx T_{\lim,\max} = 0.905 \times T_{cr} = 6880$ K is satisfied, at the temperature difference $\Delta T = T_{\ell,\max} - T_{sur} \approx 50$ K (Fig. 5). The thickness of the ejected fragment of the liquid phase is $d_2(t) \approx 30$ nm. Temperature difference $\Delta T \approx 50$ K remains for the further cases of explosive boiling as well.

Later, after the next separation of the metastable near-surface layer under the influence of laser heating, heterogeneous evaporation of the target and fragmentation, the picture of the processes is repeated. The regime of explosive boiling acquires a pulsating character (Fig. 6). Taking into account the dependence of the laser pulse on time $G(t)$ the processes of heating, evaporation and gas-dynamic expansion are of a nonstationary and non-linear nature, which affects the process of explosive boiling.

During the period of the laser pulse, the main characteristics of explosive boiling: the pressure in Fig. 7, the thickness of the ejected fragments, Fig. 8a, and the period of pulsations, Fig. 8b are widely scattered.

After the end of the laser pulse, the explosive boiling process continues at the expense of the stored thermal energy, which is promoted by a sharp increase (by 5–7 times) of the specific heat $C_p(t)$ in the critical region. The energy consumption regime slows down and acquires a quasistationary character (Fig. 6). Approximately after the 20-th boiling, the values of the temperature maxima smoothly fall off, Fig. 6, the periods of pulsations and the thickness of the ejected fragments differ little among themselves. As a result, the total amount of ejections reaches 49, and the duration of the explosive boiling process reaches $\Delta t_\Sigma \approx 20$ ns, which is several times higher than the duration of the laser pulse, $\Delta t \gg \tau$. All ejected fragments of liquid Al d_i are completely evaporated. Average time of existence of one fragment is $\Delta t_i \sim 1$ ns.

The general trend of the temporal evolution of fragments can be presented in the following form. Over time: the size of the cavity $h_i(t)$ filled with vapor is increased from 5 nm to 1.7 μm, the velocity $u_i(t)$ is increased from 0 to 2.5 km s^{-1}, the density $\rho_i(t)$ (due to cooling) is in the interval (0.65–1.38) g cm^{-3}; the pressure $p_i(t)$ and temperature $T_i(t)$ are decreased in the cavity: $p_i(t)$ from $p_{sat}(T_{\ell,\max})$ to ~ 200 bar, $T_i(t)$ from $T_{\ell,\max}$ to ~ 5400 K. The amount of melted and evaporated substance of plotted at Fig. 9 as dependencies $\delta_{liq}(t)$ and $\delta_{vap}(t) = d_\Sigma(t) + d_v(t)$, where $d_\Sigma(t) \approx 200$ nm is the part corresponding to homogeneous mechanism and $d_v(t) \approx 10$ nm is the part corresponding

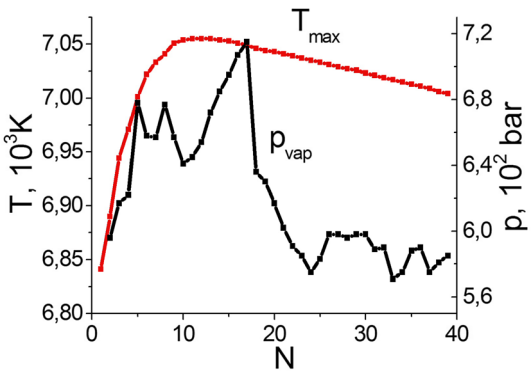

Fig. 7 The values of T_{max} in the near-surface layer of the target and pressure p_{vap} at the outer side of KL at the moments of explosive boiling

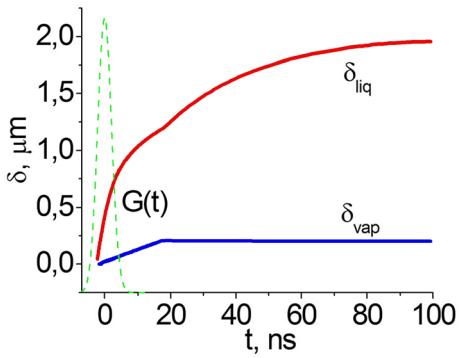

Fig. 9 Time profiles of melting depth δ_{liq} evaporated substance δ_{vap}

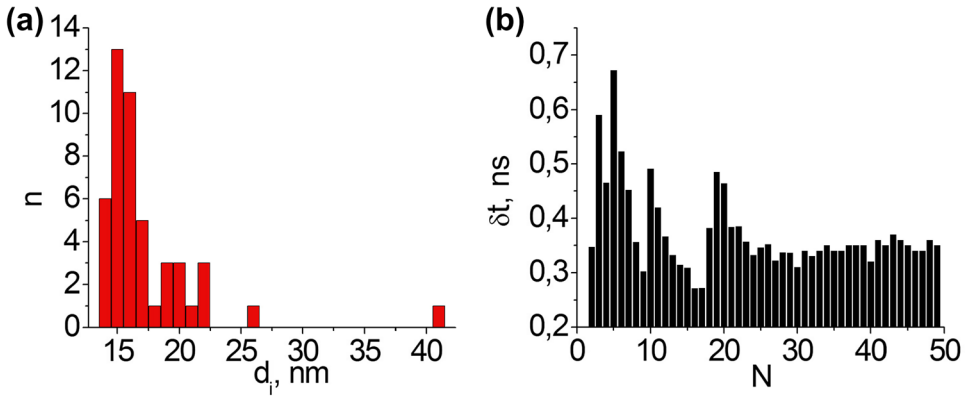

Fig. 8 The distribution of: **a** n liquid fragments of explosive boiling over linear sizes d; **b** pulsation periods between two neighbouring ejections

to heterogeneous mechanism. The process of melting turned out to be the most inertial. Due to the heat energy deposited in the liquid phase, melting continues up to the moment of $t \approx 102$ ns, when the velocity $v_{sl} = 0$. The thickness of the liquid layer reaches the maximum value $\delta_{liq}(t) \approx 2$ μm. Then the front $\Gamma_{s\ell}(t)$ turns in the opposite direction, opening the beginning of the crystallization process.

4 Conclusion

The performed mathematical modeling of the ns-laser action on the Al target made it possible to establish the principal possibility of the formation under the influence of heterogeneous evaporation and volume absorption of radiation of the temperature maximum in the near-surface layer of a superheated metastable liquid phase of a metal. The fact of reaching the ultimate superheating $T_{lim\ max}$ by the liquid phase of the metal in the near-critical region of parameters promotes the appearance of explosive boiling in the near-surface metastable layer. Thus, the mechanism of homogeneous evaporation of metals has its own characteristics, but it does not fundamentally differ from the homogeneous mechanisms for nonmetals (weakly absorbing liquids, semiconductors, dielectrics).

An approach to the formulation in the framework of the hydrodynamic model of the algorithm for simulating homogeneous nucleation in an overheated liquid phase of a metal is proposed. The classical theory of nucleation, using the assumptions of stationarity and uniformity of the temperature field, is of little use to describe homogeneous nucleation under the conditions of pulsed laser action. The approximate algorithm is based on the application in the hydrodynamic model of the quasi-nuclei of 3–5 nm thickness, the generation of which is performed by the criterion of the maximum allowable superheating of the initial region, taking into account the rapidly changing medium pressure. The criterion of the ultimate overheating is determined from the molecular dynamics simulation.

The application of the continual gas-hydrodynamic model has the advantage over atomistic models and molecular dynamics algorithms in that it makes it possible to simulate the processes of explosive boiling in spatio-temporal macroscales at relatively low computational costs.

Accounting of the temperature dependences of the thermophysical and optical properties of the metal target in the mathematical modeling made it possible to determine the regime of pulsating explosive boiling, which duration is $\Delta t_{\Sigma} \approx 20$ ns several times higher that of the laser pulse $\tau = 5 \times 10^{-9}$ s.

The simulation results showed good qualitative and quantitative agreement with the experimental data of the papers [15, 51]. In the considered regime of laser action, the total depth of the removed material due to explosive boiling ($d_{\Sigma} \approx 200$ nm) is more than an order of magnitude higher than the amount of material removed through the surface evaporation ($d_{\Sigma} \approx 10$ nm).

Acknowledgements The research was funded by the Russian Foundation for Basic Research, Grant no. 16-07-00263.

References

1. J.C. Millerin (ed.), *Laser Ablation: Principles and Applications* (Springer, Berlin, 1994)
2. D. Bäuerle, *Laser Processing and Chemistry* (Springer, Singapore, 2000)
3. C.R. Phipps (ed.) *Laser Ablation and Its Applications* (Springer, New York, 2007)
4. J. Cheng, C.-S. Liu, S. Shang, D. Li, W. Perrie, G. Dearden, K. Watkins, Opt. Laser Technol. **46**, 88 (2013)
5. R. Eason (ed.) *Pulsed Laser Deposition of Thin Films* (Wiley, Hoboken, 2007)
6. D.A. Cremers, L.J. Radziemski, *Handbook of Laser-Induced Breakdown Spectroscopy* (Wiley, New York, 2006)
7. S. Barcikowski, A. Hahn, A.V. Kabashin, B.N. Chichkov, Appl. Phys. A. **87**, 47 (2007)
8. D. Zhang, B. Gookce, S. Barcikowski, Chem. Rev. **117**, 3990 (2017)
9. V. Schmidt, M.R. Belegratis (eds.) *Laser Technology in Biomimetics: Basics and Applications. Biological and Medical Physics* (Springer, Berlin, 2013)
10. E. Fadeeva, S. Schlie-Wolter, B.N. Chichkov, G. Paasche, T. Lenarz, *Laser Surface Modification of Biomaterials, Techniques and Applications*, vol. 111 (Woodhead Publishing, Cambridge, 2016), p. 145
11. V.I. Mazhukin, A.V. Mazhukin, M.G. Lobok, Laser Phys. **19**(5), 1169–1178 (2009)
12. B. Verhoff, S.S. Harilal, J.R. Freeman, P.K. Diwakar, A. Hassanein, J. Appl. Phys. **112**, 093303 (2012)
13. A. Miotello, R. Kelly, Appl. Phys. Lett. **67**, 3535 (1995)
14. A. Mazzi, A. Miotello, J. Coll. Interface Sci. **489**, 1 (2016)
15. C. Porneala, D.A. Willis, J. Phys. D Appl. Phys. **42**, 155503 (2009)
16. N. Bulgakova, A. Bulgakov, Appl. Phys. A **73**, 199 (2001)
17. V.I. Mazhukin, A.V. Shapranov, M.M. Demin, A.A. Samokhin, A.E. Zubko, Math. Montisnigri **37**, 24 (2016)
18. V.I. Mazhukin, A.V. Shapranov, M.M. Demin, A.A. Samokhin, A.E. Zubko, Math. Montisnigri **38**, 78 (2017)
19. A.H.A. Lutey, J. Manuf. Sci. Eng. **135**, 061003 (2013)
20. V.I. Mazhukin, V.V. Nossov, I. Smurov, Appl. Surf. Sci. **253**, 7686 (2007)
21. V.I. Mazhukin, V.V. Nossov, I. Smurov, J. Appl. Phys. **101**, 024922 (2007)
22. S.S. Harilal, G.V. Miloshevsky, D.P. Kiwakar, N.L. La Haye, A. Hassanein, Phys. Plasmas **19**, 083504 (2012)
23. X.W. Li, W.F. Wei, J. Wu, S.L. Jia, A.C. Qiu, J. Appl. Phys. **113**, 243304 (2013)
24. V.I. Mazhukin, A.A. Samokhin, A.V. Shapranov, M.M. Demin, Mater. Res. Express **2**, 016402 (2015)
25. V.I. Mazhukin, A.A. Samarskii, Surv. Math. Ind. **4**, 85 (1994)
26. D. Autrique, G. Clair, D. L'Hermite, V. Alexiades, A. Bogaerts, B. Rethfeld, J. Appl. Phys. **114**, 023301 (2013)

27. G. Galasso, M. Kaltenbacher, A. Tomaselli, D. Scarpa, J. Appl. Phys. **117**, 123101 (2015)
28. H. Gleiter, Nanostructured materials: basic concepts and microstructure. Acta Metall. **48**, 1 (2000)
29. M.A. Meyers, A. Mishra, D.J. Benson, Prog. Mater. Sci. **51**, 427 (2006)
30. L.V. Zhigilei, Z. Lin, D.S. Ivanov, J. Phys. Chem. C **113**, 11892 (2009)
31. C. Wu, L.V. Zhigilei, Appl. Phys. A **114**, 11 (2014)
32. A.K. Upadhyay, N.A. Inogamov, B. Rethfeld, H.M. Urbassek, Phys. Rev. B **78**, 045437 (2008)
33. V.I. Mazhukin, A.V. Shapranov, A.A. Samokhin, A.Yu. Ivochkin, Math. Montisnigri **27**, 65 (2013)
34. N. Farid, S.S. Harilal, H. Ding, A. Hassanein, J. Appl. Phys. **115**, 033107 (2014)
35. M. Aghaei, S. Mehrabian, S.N. Tavassoli, J. Appl. Phys. **104**(5), 053303 (2008)
36. G. Clair, D. L'Hermite, J. Appl. Phys. **110**(8), 083307 (2011)
37. V.I. Mazhukin, A.V. Shapranov, M.M. Demin, N.A. Kozlovskaya, Bull. Lebedev Phys. Inst. **43**, 283 (2016)
38. V.I. Mazhukin, A.V. Shapranov, A.V. Mazhukin, O.N. Koroleva, Math. Montisnigri **36**, 58 (2016)
39. V.I. Mazhukin, A.V. .Shapranov, M.M. Demin, A.V. Mazhukin, Proc. SPIE **10453**, 104530X (2017)
40. A.A. Samarskii, P.P. Matus, V.I. Mazhukin, I.E. Mozolevski, Comput. Math. Appl. **44**, 501 (2002)
41. V.I. Mazhukin, D.A. Malaphei, P.P. Matus, A.A. Samarskii, Comput. Math. Math. Phys. **41**, 379 (2001)
42. A.V. Mazhukin, V.I. Mazhukin, Comput. Math. Math. Phys. **47**, 1833 (2007)
43. P.V. Breslavskii, V.I. Mazhukin, Comput. Math. Math. Phys. **48**, 2102 (2008)
44. B.M. Kozlov, A.A. Samokhin, A.B. Uspenskii, Kvantovaia elektronika **2**(9), 2061 (1975)
45. V.A. Batanov, F.V. Bunkin, A.M. Prokhorov, V.B. Fedorov, Sov. Phys. JETP **36**, 311 (1973)
46. Y.V. Senatsky, N.E. Bykovsky, S.M. Pershin, A.A. Samokhin, Laser Part. Beams **35**, 177 (2017)
47. B. Wu, Y.C. Shin, Appl. Phys. Lett. **89**, 111902 (2006)
48. J.E. Hatch, *Aluminum: Properties and Physical Metallurgy* (ASM, Metals Park, 1984)
49. V.I. Mazhukin, M.M. Demin, A.V. Shapranov, Appl. Surf. Sci. **302**, 6 (2014)
50. S.N. Andreev, V.I. Mazhukin, A.A. Samokhin, M.M. Demin, Kratkie soobshcheniia po fizike **7**, 50 (2006)
51. A. Spiro, M. Lowe, G. Pasmanik, Appl. Phys. A **107**, 801 (2012)